Advances in Science and Technology Research Journal

Advances in Science and Technology Research Journal, 2025, 19(1), 132–147
https://doi.org/10.12913/22998624/195277
ISSN 2299-8624, License CC-BY 4.0

Received: 2024.10.10
Accepted: 2024.11.15
Published: 2024.12.01

Analysis and prospects of efficient and precise forming technology for aeroengine turbine shafts

Xuedao Shu[1,2*], Lulu Chen[1,2], Zbigniew Pater[4], Zixuan Li[1,2], Xuhai Jie[1,2], Yingxiang Xia[1,2], Song Zhang[1,3], Qian Chen[1,2], Yongming Xu[1], Jaroslaw Bartnicki[4]

[1] Faculty of Mechanical Engineering and Mechanics, Ningbo University, Ningbo 315211, China
[2] Zhejiang Provincial Key Laboratory of Part Rolling Technology, Ningbo 315211, China
[3] College of Mechanical and Automotive Engineering, Ningbo University of Technology, Ningbo 315211, China
[4] Faculty of Mechanical Engineering, Lublin University of Technology, ul. Nadbystrzycka 36, 20-618 Lublin, Poland
* Corresponding author's e-mail: shuxuedao@nbu.edu.cn

ABSTRACT

The turbine shaft is a crucial core component of aeroengines, made of difficult-to-deform high-temperature alloy materials, characterized as a long hollow stepped shaft with deep internal holes. Achieving efficient, high-performance, and precise manufacturing of turbine shafts is a cutting-edge issue urgently needing resolution in the field of aeroengine manufacturing. Currently, the forming process for turbine shafts mainly involves forging the external shape, followed by machining the outer profile and drilling the internal holes, which presents problems such as low efficiency and high material consumption. This paper analyzed the principles and characteristics of advanced forming processes for shaft components, including cross-wedge rolling (CWR), three-roll skew rolling (TRSR), as well as piercing and cross rolling integration (PCRWI). This paper expounded the principles and characteristics of these process forming turbine shafts. The research results show that the short-process flexible forming method of piercing-rolling integration can make the outer profile and inner hole of the turbine shaft synchronously formed. This process can effectively realize the high-quality, high-quality and efficient production of the turbine shaft. Therefore, this process is the development direction of accurate plastic forming of aeroengine turbine shaft. The research results have significant theoretical value and practical engineering implications for enhancing the overall manufacturing capability of aeroengines.

Keywords: turbine shaft; cross-wedge rolling; three-roll skew rolling; piercing and rolling integration; flexible forming.

INTRODUCTION

Aeroengines are usually used in harsh environments such as high temperature and high pressure [1, 2]. As shown in Figure 1, the turbine shaft is a key component to ensure the normal operation of the engine. With the rapid development of the aviation industry, the demand for high-quality turbine shafts is increasing rapidly. In order to manufacture high-quality aeroengine turbine shafts, scholars at home and abroad have studied its forming and manufacturing technology from multiple perspectives. Jang DY et al. [3] from Korea developed an elastic-plastic nonlinear finite element model of radial forging of turbine shaft,

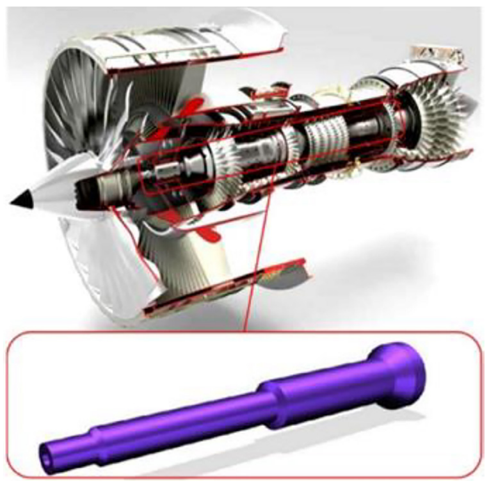

Figure 1. A certain type of aero-engine turbine shaft

elucidating the distribution of residual stresses in forged products. Duan et al. [4] investigated the effects of three process parameters, namely initial temperature, final forging temperature and forging speed, on the wear resistance performance of GH901 high-temperature alloy turbine shafts. They determined that the optimal combination for maximizing wear resistance is an initial temperature of 1200 °C, a final temperature of 920 °C, and a forging speed of 10 mm/s. Tan et al. [5] compared the high and low structure and mechanical properties of turbine shaft forgings forged by two forming processes of ' pier head-pulling rod ' and ' forging-drawing-pier head '. The high and low structure of forgings is shown in Figure 2. The grain size of method two is obviously smaller than that of method one, and the grain distribution of method two is more uniform than that of method one. Therefore, the microstructure, properties and qualification rate of method two forgings are higher than that of method one. Liu [6]proposed the forming process of low-pressure turbine shaft integral forgings, which solved the phenomena of bending, warping and eccentricity of the rod in the conventional forging process. Wang [7] divided the disc and shaft parts of the GH4169 alloy turbine shaft into two-step forging. By adjusting the appropriate precision forging temperature, the overall comprehensive performance of the forgings for two-step forging is good.

It is also very important to realize the accurate machining of the remaining amount after the turbine shaft is formed. Ding [8] studied the variation of the axial force and torque of the tool under different drilling parameters in cutting the outer profile of the turbine shaft. It was concluded that the feed rate has a great influence on the axial force and torque, and the spindle speed has little influence on the axial force and torque. When the spindle speed is 170 and the feed rate is 0.06, the axial force and torque are the smallest. Yao et al. [9] studied the turning process of slender turbine shafts for a certain aircraft, focusing on machining techniques, tool selection, and process flows. They proposed improvement measures for the existing process challenges and validated them through experiments. Wang Lian et al. [10] focused on the machining of the inner bore and outer contour of low-pressure turbine shafts using a thin-walled hollow long shaft from a batch production model as the research object, and they achieved this by reasonably arranging the machining process route. Chen [11] designed and manufactured special deep-hole drills, deep-hole reamers, and other specialized tools, as well as CNC clamping tools. They sought the optimal tool path and tool entry point positions, adjusted and optimized the CNC programs, and explored the best cutting parameters, which were validated through cutting tests to confirm the accuracy and rationality of the CNC programs. Ma et al. [12] analyzed the deformation characteristics of the turbine shaft during the cutting process, and determined the mechanical model of the workpiece. The deformation and stress of the workpiece are shown in Figure 3. One end of the workpiece is clamped with a chuck, and the other end is supported by the top of the lathe tailstock. Under the action of cutting force, the workpiece presents bending deformation. When cutting the outer contour of the turbine shaft, the resonance phenomenon will be caused and the forming quality of the turbine shaft will be reduced. The structure of the turbine shaft is simplified as necessary. The structural mode of the turbine shaft is determined by the characteristics of the structure itself and the material properties, and has nothing to do with the external load. The forced vibration under

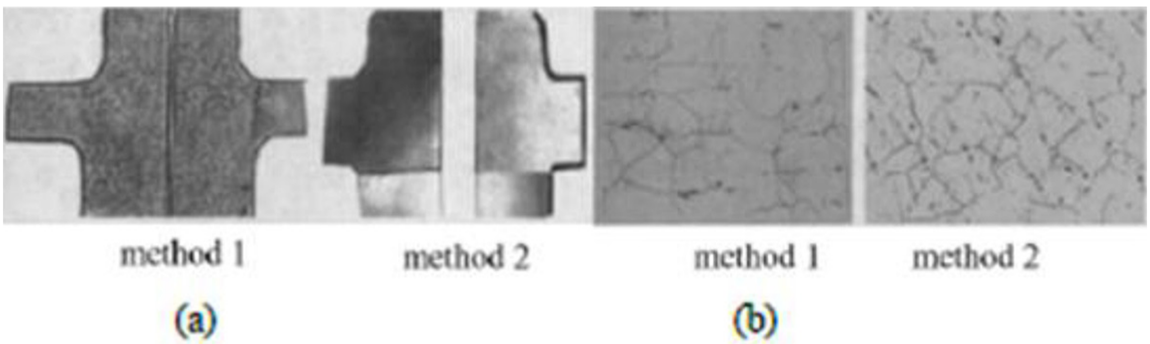

Figure 2. Forging structure (Reprinted from ref.5). (a) Forged low-magnification microstructure (×0.5), (b) Forged high-magnification microstructure (×100)

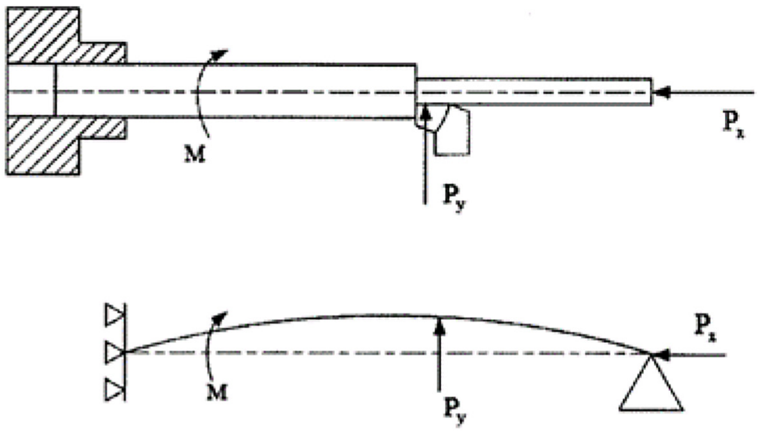

Figure 3. Deformation and stress of turbine shaft (Reprinted from ref.12)

the condition and the external load can be linearly composed according to the forced vibration of these basic characteristics. The mathematical model is the second-order simultaneous differential equation in the following form (1)

$$M\ddot{\delta}(t) + C\dot{\delta}(t) + K\delta(t) = P_Q(t) \quad (1)$$

where: M is the system structure quality matrix; K is the stiffness matrix of the system structure; M K are usually a real coefficient symmetric matrix, C is the damping matrix of the system structure (an asymmetric matrix); $\delta(t)$ is the displacement response of each point of the system; $P_Q(t)$ is the excitation force vector of the system.

The machining of the inner hole of the turbine shaft has always been one of the difficulties in the machining of shaft parts[13][14][15]. The machining process of the inner hole of the turbine shaft is drilling and boring guide hole-drilling-reaming-boring. Drilling and boring the guide hole can increase the rigidity of the drill bit, play a guiding role, and prevent the hole from deflecting. Reaming can further remove the machining allowance and prepare for finishing. Repeated boring in the inner hole to repair the deformation after heat treatment and reduce the thickness difference be-tween the inner and outer walls of the shaft. Feng et al. [16] analyzed the material characteristics, the structural characteristics of the parts and the processing difficulties, formulated the process flow, and used the orthogonal test design method to carry out the deep hole drilling test on the low-pressure turbine shaft of GH4169 nickel-based superalloy, and obtained a reasonable combination of drilling process parameters: spindle speed 170, feed rate 0.06, cutting fluid flow 110. Ding8designed a mixed horizontal orthogonal test, and analyzed the influence of drilling parameters on the experimental machining, chip morphology, tool wear and hole axis deflection. The better drilling parameters were obtained by comprehensive evaluation: spindle speed 170, feed rate 0.06. Wang [17] took a certain type of high-pressure turbine rear shaft as the test object, improved the processing technology of aeroengine high-pressure turbine rear shaft parts, and introduced the turn milling composite processing technology. The principle of turn-milling composite processing technology is to process the turning part and the milling part together as much as possible in a clamping station, reduce the number of processes, and then control the number of turnovers, avoid repeated clamping of parts, and realize the turn-milling integrated processing of high-pressure turbine rear shaft parts. The processing can be shortened from the original 42 to 27. Luo [18] analyzed the machining process of the high-pressure turbine rear shaft in aeroengines, introduced the machining equipment as well as material characteristics, and identified the key challenges in machining while optimizing the process. Jiang [19] designed an ultra-long solid carbide boring bar with a length-to-diameter ratio of 15 and a length exceeding 1 meter, addressing the limitations of traditional internal bore machining methods in the deep-hole boring of hollow long shafts with a slenderness ratio greater than 10. Liu et al. [20] modified the structure of the turbine shaft of the original turbine drill and conducted actual drilling operations, confirming the feasibility of machining large-diameter deep holes using the CA-2-1 type pipe thread lathe. The research above indicates that the current primary process for forging the stepped shaft shape of turbine shafts involves subsequent deep processing of inner holes. However, existing manufacturing processes face several challenges, including cumbersome forming procedures, lengthy processes, difficulty in deep processing the inner holes of long shafts, fiber cutting reducing metal performance, low production efficiency, and material utilization rates. To achieve high-quality and high-volume production of aeroengine turbine shafts, this paper analyzed the principles and characteristics of advanced shaft forming technologies, such as CWR, three-roll skew rolling (TRSR), as well as PCRWI. It discussed key issues and the feasibility of these processes in shaping turbine shafts. The study identified that the integrated short-process flexible forming method of PCRWI represents the future direction for precise plastic forming of aeroengine turbine shafts, providing technical guidance to advance the global aviation industry.

Feasibility analysis of forming turbine shaft by cross wedge rolling

Multi-wedge synchronous cross-wedge rolling

Multi-wedge synchronous special rolling is a kind of advanced forming technology for shaft part [21][22]. This process involves the use of multiple wedge-shaped molds to simultaneously achieve radial reduction and axial extension of the rolled material. The technique employs two rolls, each equipped with a series of wedge-shaped molds, which rotate in the same direction. This rotation drives the circular workpiece to spin, facilitating the desired shaping through the combined actions of radial compression and axial elongation. The rolling piece is rolled into shaft parts of various shapes and lengths under the action of wedge-shaped pass. The deformation of cross wedge rolling is mainly radial compression and axial extension. During rolling, the radial force from the rolls compresses the workpiece radially, while the tangential friction drives the workpiece rotation, ensuring continuous radial deformation. Because the rolled piece is deformed in the roll pass, the rolled piece is also subjected to an axial force, which promotes or prevents the rolled piece from extending deformation. Under the action of these external forces, the deformation process and metal flow law inside the rolled piece are very complex, and in the process of multi-wedge synchronous special rolling, there is still a complex mutual restriction relationship between the wedges, resulting in the mold design process. The calculation of the deflection angle is complicated, as shown in formula (2) [23]. It is evident that there are many design parameters of deflection angle. If the selection is not appropriate, the phenomenon of rolling uncleanness appears on the long shaft section with equal diameter, as shown in Figure 4. Therefore, the key of multi-wedge rolling long shaft hollow turbine shaft is how to ensure the smooth metal transition between wedge.

$$\tan\theta_3 = \begin{cases} \dfrac{\tau^2 \tan\alpha_1 \tan^2\beta_1}{3\pi(r_0^2 - r_0'^2)} + \dfrac{\tau^2 \tan\alpha_2 \tan^2\beta_{21}'}{3\pi(r_0^2 - r_0'^2)} & \text{(Both the first and second wedges are wedged)} \\ \dfrac{\tau^2 \tan\alpha_1 \tan^2\beta_1}{3\pi(r_0^2 - r_0'^2)} + \dfrac{r_0^2 - r_1^2}{r_0^2 - r_1'^2}\tan\beta_{21}' & \text{(The first wedge is wedged, and the second wedge is widened)} \\ \dfrac{r_0^2 - r_1^2}{r_0^2 - r_1'^2}\tan\beta_1 + \dfrac{\tau^2 \tan\alpha_2 \tan^2\beta_{22}'}{3\pi(r_0^2 - r_0'^2)} & \text{(The first wedge is widened, and the second wedge is wedged)} \\ \dfrac{r_0^2 - r_1^2}{r_0^2 - r_1'^2}\tan\beta_1 + \dfrac{r_0^2 - r_1^2}{r_0^2 - r_1'^2}\tan\beta_{22}' & \text{(Both the first and second wedge are widened)} \end{cases} \quad (2)$$

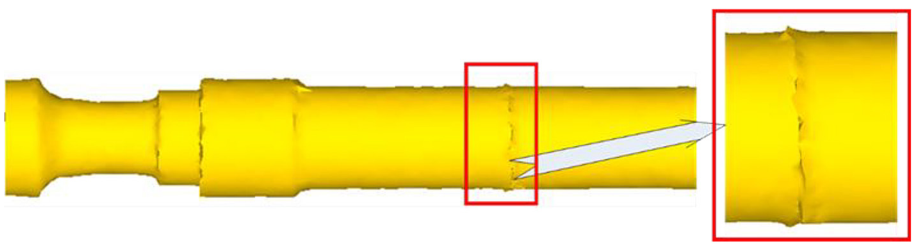

Figure 4. The unrolled portion of the long shaft section with a constant diameter

where: θ is the deflection angle; τ is the distance the rolled piece travels along the mold roller surface; t is the amount of movement at the end of the rolled piece; α is the forming angle; β, β'_{21}, β'_{22} are the spreading angles, the actual spreading angle of the second wedge entry segment, the actual spreading angle of the second wedge spreading segment; r_0, r_0' are the initial outer diameter and initial inner diameter of the rolled piece; r_1, r_1' are the outer diameter and inner diameter of the rolled piece after forming.

In multi-wedge rolling forming, due to the uneven flow velocity of the inner and outer parts of the metal, a certain deflection angle must be selected for the mold for ease of machining. This results in the side wedge not being able to avoid the metal in time during the initial stages of the wedge entry and spreading segments, causing the step section to be compressed. In the later stages of the spreading segment and before the finishing segment, the metal flow rate cannot keep up with the mold deflection speed, leading to the middle long shaft section with a constant diameter being stretched, resulting in wall thickness reduction and uneven wall thickness. To address this, the wedge of the mold transition section is modified using a rolling curve. As shown in Figure 5, the transition is evidently smooth, and the forming effect is quite good, effectively controlling the surface quality of the long hollow shaft.

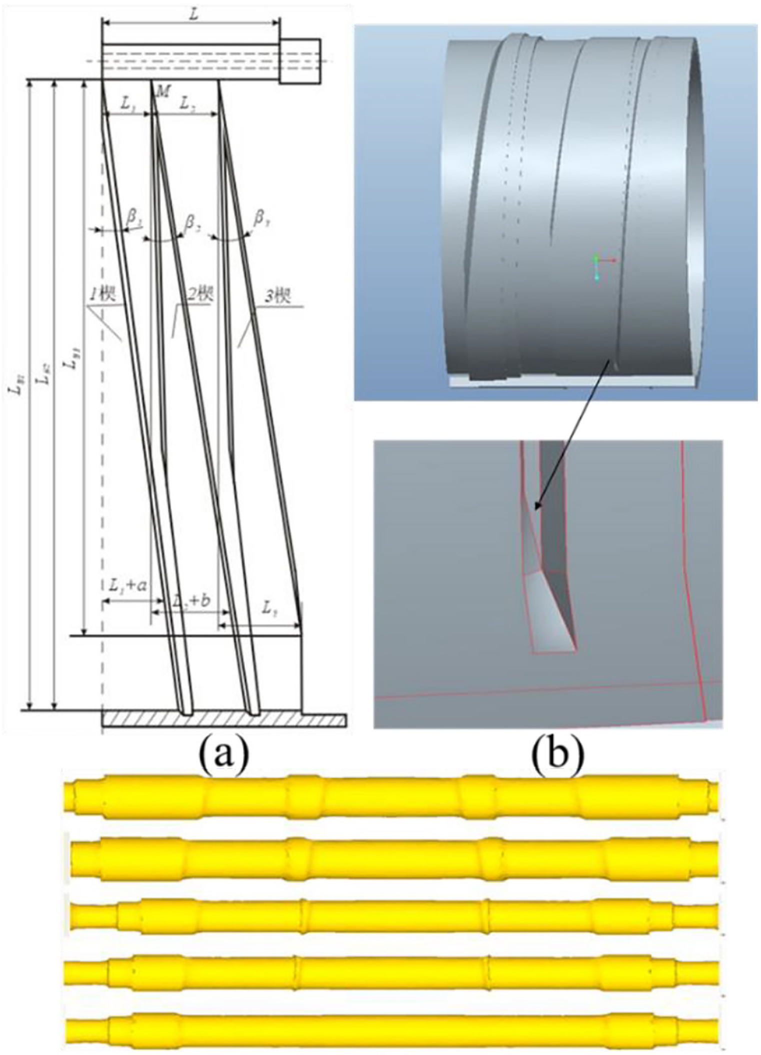

Figure 5. Mold design scheme and the forming process of the smooth transition section of the three-wedge long shaft (a) multi-wedge die, (b) three-dimensional model of multi-wedge die, (c) transition section forming diagram.

Multi-wedge cross rolling for synchronous rolling of long hollow shafts ensures consistent internal diameters by inserting a core rod into the heated rolled billet. This method results in a more complex layout than conventional wedge cross rolling. By developing a mechanical model for multi-wedge synchronous rolling of hollow train axles, Zheng [24] derived the conditions for stable rolling and established the criteria for wedge cross-rolling instability that lead to the flattening of the hollow train axle. The schematic diagram of automated multi-wedge synchronous cross rolling for hollow shafts is shown in Figure 6. Consisting primarily of heating equipment 1, hollow billet 2, conveyor rollers 3, variable-angle inclined stands 4, core rod insertion device 5, wedge cross rolling machine 6, formed piece 7, and core rod extraction device 8. The billet overturning machine and inclined stands are integrated into a variable angle inclined stand design. This layout ensures equipment support for multi-wedge synchronous technology in forming turbine shafts. Through optimized mold parameters, multi-wedge synchronous cross rolling technology for forming turbine shafts is feasible.

Combined cross wedge rolling forming technology

Aiming at the problems of large die diameter, large equipment and high cost in the process of forming large shaft parts by single wedge cross wedge rolling, Pater proposed a multi-roll combined cross wedge rolling method. As shown in Figure 7 [25][26], the multi-roll combined cross wedge rolling divides the rolling process into two stages. Initially, the left and right rolls in each set of rolls are individually spaced apart from the central rolls. Subsequently, the heated blank is advanced axially through the gap between the intermediate rolls of the three distinct roll groups. This precise alignment and movement ensure the controlled deformation of the material as it passes through the rolling process. Then, the rotation of the intermediate rolls is controlled in the three sets of rolls, the intermediate section of the billet is rolled, stopping after the intermediate roll rotates one circle, and the intermediate section of the billet is rolled. The left and right rolls in each set are connected coaxially to the intermediate rolls and are driven to rotate synchronously by them for one complete revolution. The intermediate rolls are used to finish the middle section of the billet. At the same time, the left and right rolls are rolled at both ends of the billet to obtain the rolled piece. The advantage of this method is that it can greatly reduce the size of the combined roll mold and the size of the whole machine, which can save at least 1/3 of the mold space, and ensure the forming quality of large long shaft parts. Figure 8 is a hollow shaft with different wall thickness rolled by the combined cross wedge rolling forming technology [27]. Compared with the traditional process, the hollow axle produced by this technology has high dimensional accuracy, good surface finish, smooth surface of the rolled piece, and no obvious defects, such as depressions and cracks. This suggests that the combined wedge

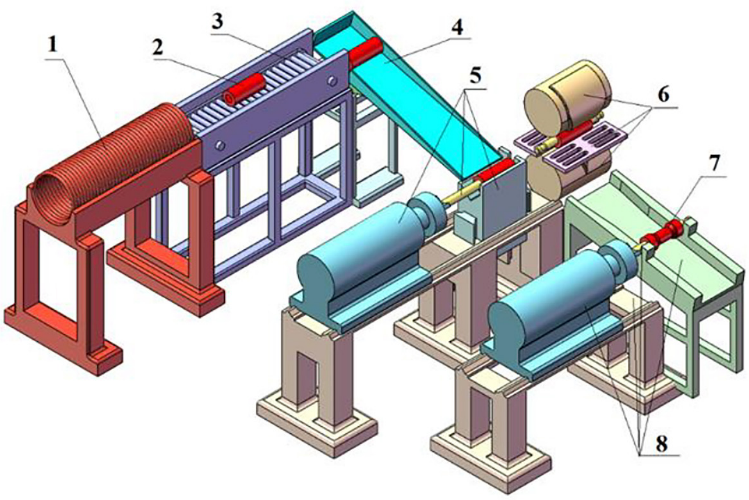

Figure 6. Schematic of rolling line: 1. Heating equipment, 2. Hollow billet, 3. Conveyor rollers, 4. Variable-angle inclined stand, 5. Core rod insertion device, 6. Cross wedge rolling machine, 7. Formed piece, 8. Core rod extraction device

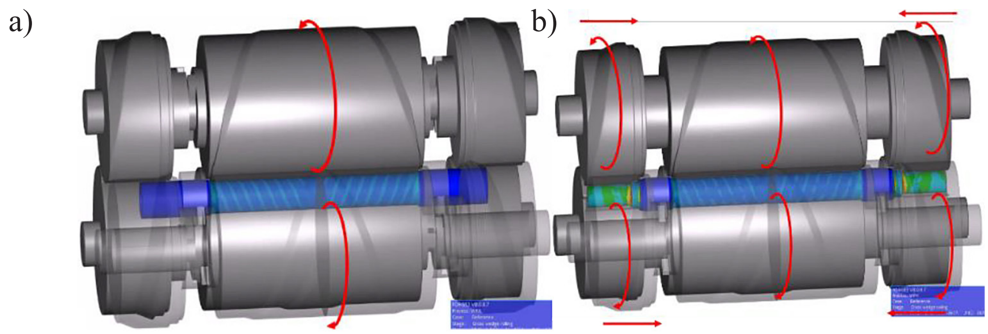

Figure 7. Combined cross wedge rolling process: (a) rolling of an intermediate wedge (b) rolling of side wedges

Figure 8. Hollow shaft formed by rolling

cross-rolling technology can be applied to the manufacturing of turbine shafts.

Flexible forming principle of three-roll cross rolling

As shown in Figure 9 [28], it is a schematic diagram of the three-roll skew rolling (TRSR) forming principle for a turbine shaft. The three rollers rotating in the same direction are distributed around the rolling center line at a circumference of 120°120°, and the roll axis is deflected by a certain angle relative to the rolling center line (i.e. the feed angle)[29]. In the rolling process, the three same rolls rotate in the same direction around their respective axes, and drive the rolling piece to rotate in the opposite direction. Due to the existence of the feed angle, the rotation of the roll can provide axial force for the rolling piece, thus driving the rolling piece to move along the axial direction. Controlling the roll spacing of the three rolls can achieve the flexible forming requirements of the multi-step turbine shaft, whereas the traction of the chuck can regulate the rolling speed and stability.

Feasibility analysis of three-roll cross rolling based on hollow billet turbine shaft

The superalloy turbine shaft installed on the turbine rotor of an aero-engine is taken as the research object, and the size is reduced according to the ratio of 1: 3. The specific size is shown in Figure 10. According to the principle of equal volume, and appropriate to leave a certain amount of processing residue, the final selection of outer diameter 50 mm, inner diameter 10 mm, length 230 mm tube blank rolling. The three-dimensional geometric models of turbine shaft tube blank, roll, mandrel and chuck were established by using Solidworks software, and these models were saved as STL format. Then, the STL file was imported into Simufact finite element software, and finally the finite element model of three-roll skew rolling (TRSR) of turbine shaft was established as shown in Figure 11 [30]. In Simufact preprocessing, the

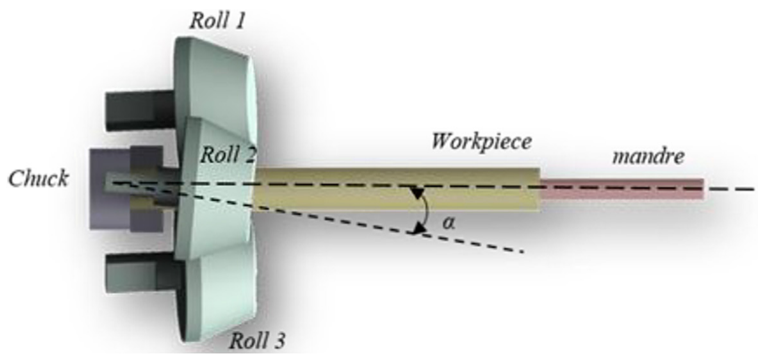

Figure 9. Schematic diagram of three-roll skew rolling principle of turbine shaft

material for the tube billet is set to GH4169 high-temperature alloy, which is commonly used for key components in aircraft engines due to its high strength and excellent corrosion resistance [31] [32]. During the simulation process, the physical properties of the material were set as follows: thermal conductivity: 11.4$W \cdot m^{-1} \cdot K^{-1}$, specific heat capacity: 435$J \cdot kg^{-1} \cdot K^{-1}$, thermal expansion coefficient: $1.3 \times 10^{-5} K^{-1}$, Young's modulus: 203$GPa$, Poisson's ratio: 0.29, density: 8190$kg \cdot m^{-3}$. The simulation parameters are shown in Table 1.

Through the point displacement tracking function of the Simulation software, the flow law of the metal on the rolled piece was explored. In the direction of the rolling line on the rolled piece, a total of 9 sections from 'A' to 'I' were intercepted equidistantly, of which section 'A' and section 'E' were 23 mm away from the left and right ends of the billet, respectively. Five sampling nodes were defined from the inside to the outside along the radial direction on each section, marked as P1-P5, and the position of the sampling nodes was shown in Figure 12. Figure 13 is the displacement cloud diagram of the final forming of the rolled piece, in which the cross section is the cutting diagram of the rolled piece along the direction of the rolling line. It can be seen from the figure that the axial displacement of each section node gradually decreases from the inner surface to the outer surface along the radial direction. Along the axial direction, it gradually increases from left to right, and the amplitude of the increase gradually increases. Therefore, it is shown that the metal of the turbine shaft mainly flows along the axial direction during the TRSR forming process. To investigate the out-of-roundness and wall thickness uniformity

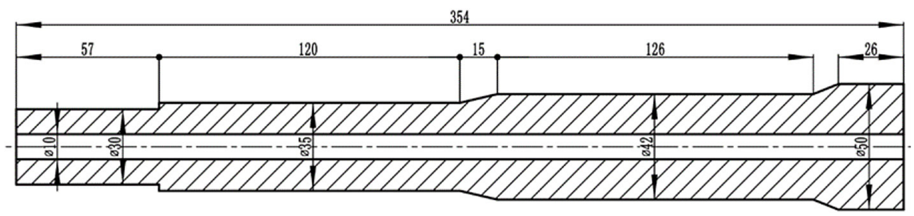

Figure 10. Turbine shaft size diagram 1:3

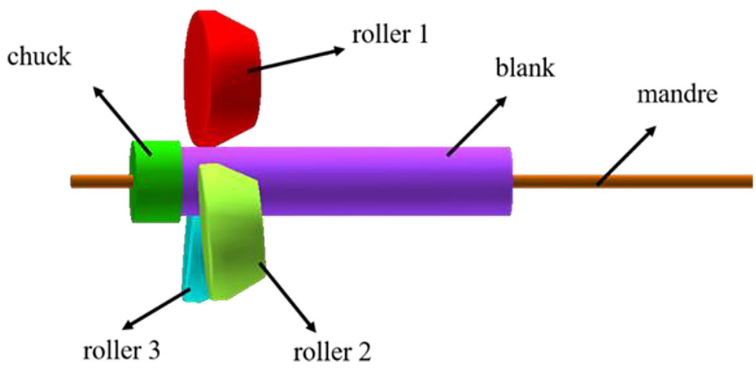

Figure 11. Finite element model of three-roll cross rolling of turbine shaft

Table 1. Process parameters for numerical simulation

Process parameters	Value
Rotation speed of the first pass n_1	80 rad·min^{-1}
Axial speed of the first pass v_1	20 mm·s^{-1}
Rotation speed of the second pass n_2	60 rad·min^{-1}
Axial speed of the first pass v_2	20 mm·s^{-1}
Feed angle α	5°
Thermal conductivity coefficient	0.05 kW / (m^2 · K)
Thermal emissivity	0.25
Friction coefficient between the workpiece and the roller	0.9
Friction coefficient between the mandrel and the workpiece	0.1
Initial preheat temperature of the billet	1050 ℃
Ambient temperature	20 ℃
Die temperature	150 ℃

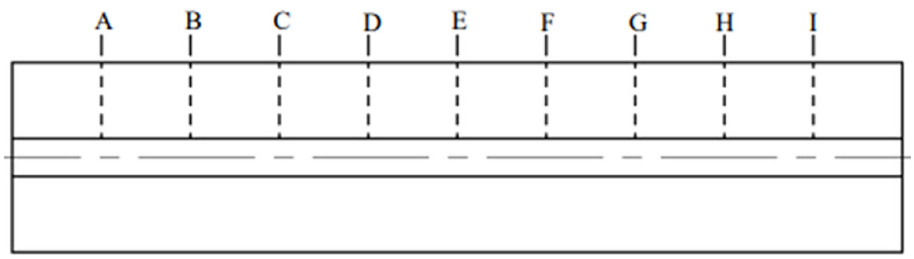

Figure 12. Metal flow sampling node position

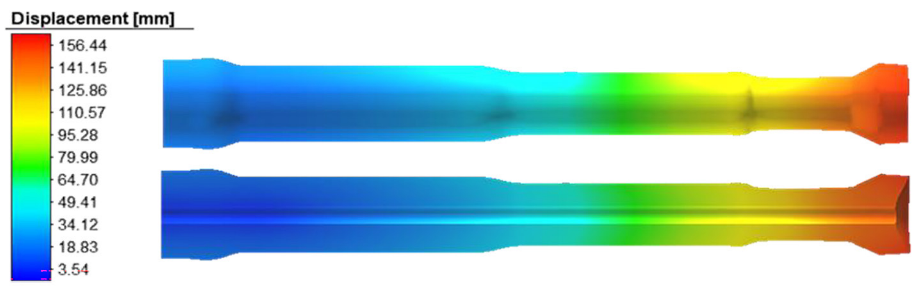

Figure 13. The displacement distribution of the final rolled piece

errors of a turbine shaft, three sections with equal diameters, created by the rollers on the shaft, were chosen as the subjects of the study. In the turbine shaft, which consists of three constant diameter sections from left to right, 7 cross-sections were selected for the first section, 7 for the second section, and 4 for the third section, totaling 18 cross-sections for the three sections, and 21 sampling nodes corresponded to the inner and outer rings of each section (as shown in Figure 14.). The out-of-roundness error was calculated by using the least squares circle method, and the wall thickness standard deviation represented the wall thickness uniformity. The roundness error was determined using the least squares circle method. Specifically, this involved calculating the coordinates of the circle's center (a, b) (The formula for calculating the center of the circle is shown in (3).) and the radius $\boldsymbol{R}$ to minimize the sum of the squared distances from the sampling points to the circle (as it was shown in Equation (4)). The roundness error was then defined as the difference between the maximum distance R_{max} and the minimum distance R_{min} from the sampling points to the circle's center. The calculation formula is provided in (5). The wall thickness standard deviation was computed based on the variation in wall thickness measurements obtained from the sampling

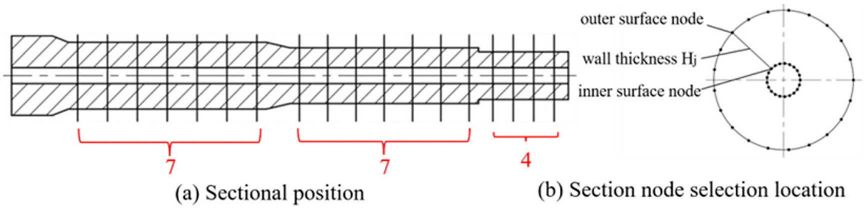

Figure 14. Sampling point location

points, providing a measure of the uniformity of the wall thickness across the cross-section. The calculation formula is provided in (6). Figure 15 shows the curve of 18 sections forming quality change. It can be seen from the diagram that the variation trend of the outer roundness error and the wall thickness standard deviation of the rolled piece from left to right section is basically the same. The maximum values of the first step and the second step are located in the last section of the step. The maximum values of the outer roundness error and the wall thickness standard deviation of the first step are 0.219 mm and 0.057 mm. The maximum values of the second step are 0.165 mm and 0.050 mm, respectively. The roundness error and wall thickness standard deviation of the 16th and 17th sections on the rolled piece are smaller than those of the other sections. This is because the metal in this area is subjected to axial tensile stress and flows along the axial direction, thereby reducing the additional deformation of the metal. Therefore, the two sections at the necking position have better roundness and wall thickness uniformity. Therefore, the feasibility of forming turbine shaft by this process is theoretically explained.

$$\begin{cases} a = \frac{2}{n}\sum_{i=1}^{n}(r_i\, cos\theta_i) \\ b = \frac{2}{n}\sum_{i=1}^{n}(r_i\, sin\theta_i) \\ R' = \frac{2}{n}\sum_{i=1}^{n} r_i \end{cases} \tag{3}$$

$$F\left(a, b, R'\right) = \sum_{i=1}^{n}(R_i - R')^2 = \sum_{i=1}^{n}\left(\sqrt{(x_i - a)^2 + (y_i - b)^2} - R'\right)^2 \tag{4}$$

$$\delta = R_{max} - R_{min} \tag{5}$$

where: n is the number of sampling points on the cross-section; (r_i, θ) is the polar coordinates of the sampling points; i is the index of the sampling points, (a, b) is the center and the radius; R' is the least squares circle

$$\begin{cases} H_j = \sqrt{(x'_j - x_j)^2 + (y'_j - y_j)^2} \\ \overline{H_j} = \frac{1}{n}\sum_{j=1}^{n} H_j \\ \sigma_j = \sqrt{\frac{1}{n}\sum_{j=1}^{1}(H_j - \overline{H_j})^2} \end{cases} \tag{6}$$

where: (x'_j, y'_j) is the coordinate value of the *jth* node of the outer ring of the section; (x_j, y_j) is the coordinate value of the *jth* node of the inner ring of the section; j is the serial number of the section node; H_j is the average wall thickness of the section; n is the number of wall thickness on each section.

The team led by Szota PL at the Czestochowa University of Technology in Poland provided a detailed theoretical and experimental explanation of the forming process of aluminum rods using

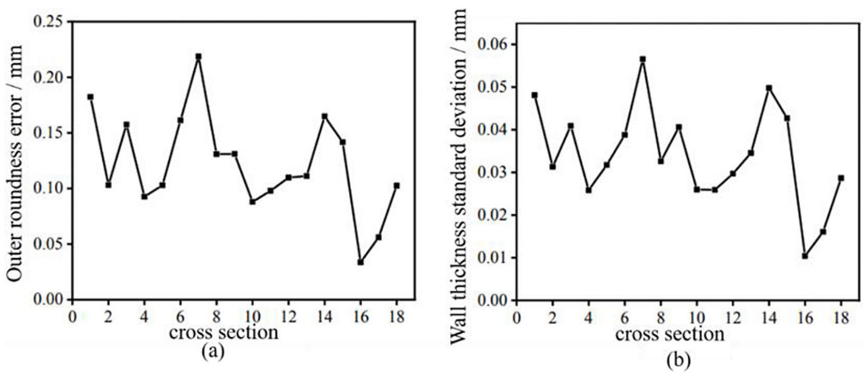

Figure 15. Variation of section forming quality; (a) outer roundness error (b) wall thickness uniformity

three-roll skew rolling. They also investigated the influence of process parameters on the temperature field of the rolled workpiece during the three-roll skew rolling process [33][34]. To further validate the process, rolling experiments were carried out in the part forming laboratory of the Technical University of Lublin, Poland, using a Ti6AIAV hollow axle as the research abject. The forming process is shown in Figure 16 [35][36][37]. Firstly, the billet was heated to 980 °C using the heating furnace, and then the high-temperature hollow shaft blank was secured onto the four-jaw chuck. Afterwards, the rolled piece was inserted into the roll gap through the axial feed mechanism; then, the roll and the fixture moved simultaneously to form a hollow shaft. The axial traction speed of the fixture and the radial feed speed of the roll were controlled by the control system to form. Finally, the rolled piece was taken out of the fixture and cooled by water. Figure 17 shows the temperature field simulation of the three-roll skew rolling of a hollow shaft obtained using the finite element simulation software Simufact (The roll speed is 60 rad/min, the feed angle is 7°, the axial traction speed is 40 mm/s, the friction coefficient between the roll and the rolled piece is 0.9, whereas the heat transfer coefficient between the workpiece and the mold is 20 kW/m²·K.). The experimentally rolled piece matched the simulation results in terms of geometry and features, validating the effectiveness of the rolling process.

Integrated piercing-rolling forming of aviation turbine shaft

Forming principle and characteristics

Figure 18 is the forming process of PCRWI. Firstly, the solid bar was heated and entered into the perforation area composed of the two rollers and the piercing plug for solid perforation to form a hollow tube blank, and the inner hole forming of the hollow shaft could be completed without machining (short process). Subsequently, the cross-rolling area composed of flexible rolls was entered for flexible rolling with self-adjusting shape consistent with the shape of the shaft, and the shaft shape forming (flexible forming) could be completed without the

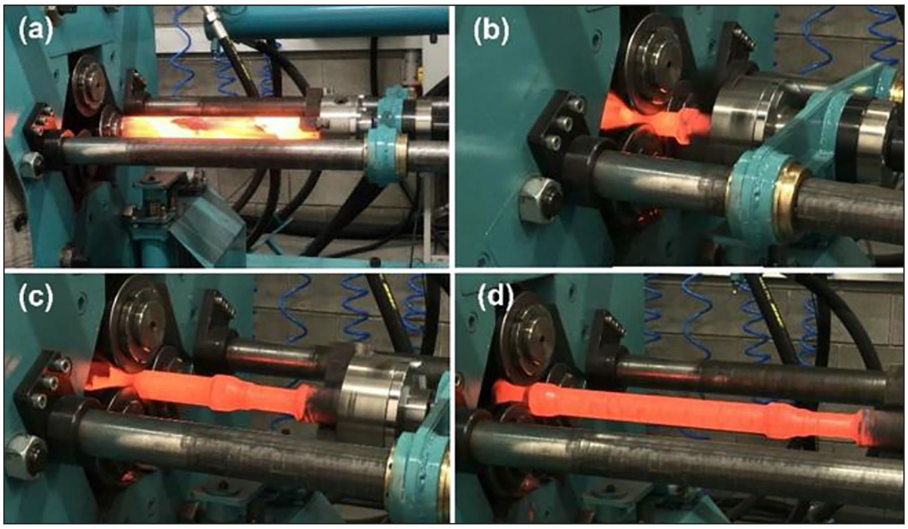

Figure 16. Forming process of hollow shaft three-roll cross rolling experiment: (a) feeding, (b) initial rolling, (c) rolling in progress, (d) rolling completed

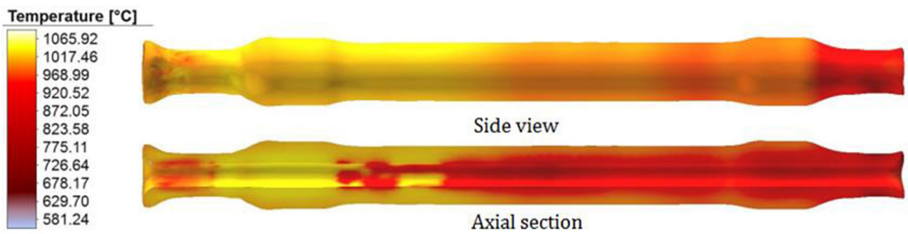

Figure 17. Temperature field simulation diagram of three-roll cross rolling hollow shaft forming process

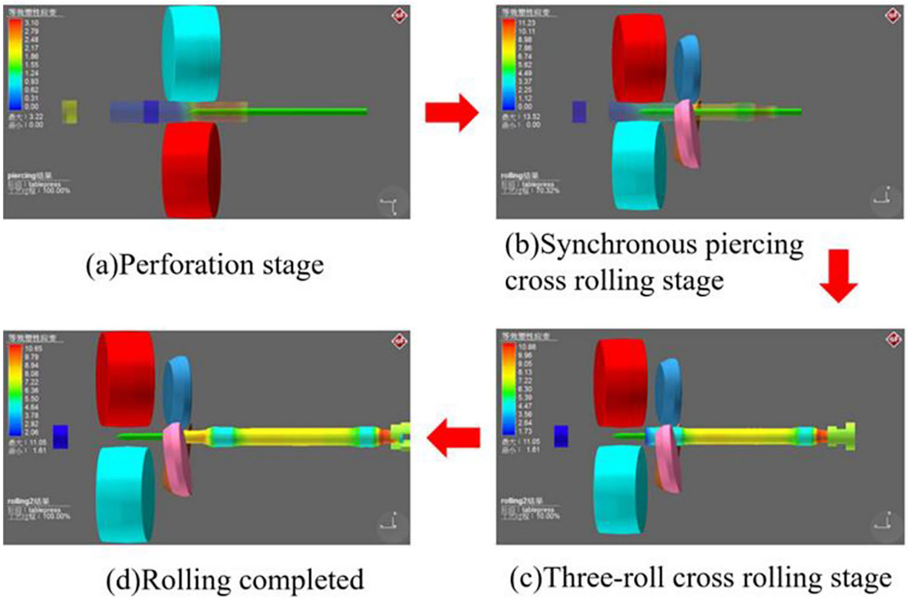

Figure 18. Integrated forming process of piercing and cross rolling

mold; precise forming could be achieved through the coordinated control of rolling and rolling. The process of forming hollow shaft by this process can be divided into four stages: piercing stage, synchronous piercing stage, TRCR stage and rolling completion. Because the hollow shaft piercing and rolling synchronous forming is to complete the inner hole forming and the step shape forming in one process, there is no need to carry out the deep processing of the inner hole alone, the process is short, the material waste is avoided and the continuity of the metal rolling fiber is maintained, which is beneficial to improve the mechanical properties of the aluminum alloy hollow shaft, meet the production of diversified parts, and reduce the production and manufacturing costs [38][39].

Forming process and quality control

Figure 19 shows a three-dimensional geometric model of turbine shaft piercing and skew rolling integration [40]. The model is mainly composed of turbine shaft blank, three groups of rolls, ejector rod, push block and positioning ring. It was imported into Simufact finite element simulation software for simulation test. Simulation parameters were set as shown in Table 2. The strain field distribution of the longitudinal section of the rolled piece and each important cross section of the deformation zone are shown in Figure 20. On the first step shaft section (section 1-1, section 2-2), the strain started from the outer surface and gradually penetrated inward. The strain on the inner surface was small and the overall strain was basically the same. On the second step shaft section (section 3-3, section 4-4), the outer surface strain increased rapidly with the reduction deformation, and no longer continued to increase after the strain reaches 4.60. The change process of the inner surface was relatively slow due to the resistance of the ejector rod. On the third step shaft section (section 5-5, section 6-6), the outer surface strain continued to increase to a maximum of 15.34, while the inner surface strain remained unchanged. In general, the outer surface strain was larger than the inner surface in the process of PCRWI, indicating that the metal flows from the outer surface to the inner surface during rolling. The strain of the reducing section was larger than that of the piercing section, and the strain of the cross section of the rolled piece shows a more regular annular distribution. Select feed angles and speeds for the piercing roll (feed angles: 6°, 8°, 10°; speeds: 40 rad/min, 60

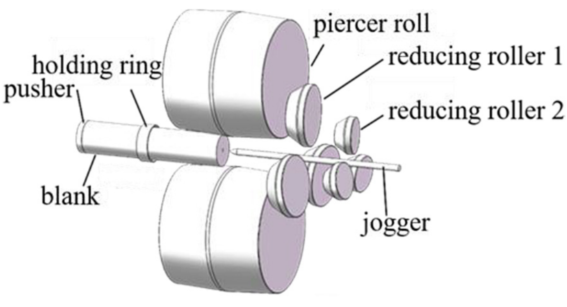

Figure 19. Piercing-rolling integrated finite element simulation model

rad/min, 80 rad/min); feed angles and speeds for the reducing roller 1 (feed angles: 7°, 9°, 11°; speeds: 90 rad/min, 110 rad/min, 130 rad/min); feed angles and speeds for the reducing roller 2 (feed angles: 8°, 10°, 12°; speeds: 110 rad/min, 130 rad/min, 150 rad/min) to design a six-factor and three-level orthogonal experiment, comprising a total of 27 trials, to study the effect of process parameters on the outer diameter error, outer roundness error, and wall thickness variance of the turbine shaft. The test results are shown in Figure 21 [41]. The orthogonal test results were

Table 2. Simulation process parameters

Process parameters	Values
Piercing roll feed angle α_1/°	6
Piercing roll rotational speed n_1/rad·min^{-1}	60
First-pass reduction roll feed angle α_2/°	9
First-pass reduction roll rotational speed n_2/rad·min^{-1}	90
Second-pass reduction roll feed angle α_3/°	12
Second-pass reduction roll rotational speed	150
First-pass reduction amount/mm n_3/rad·min-1	
Second-pass reduction amount/mm	11

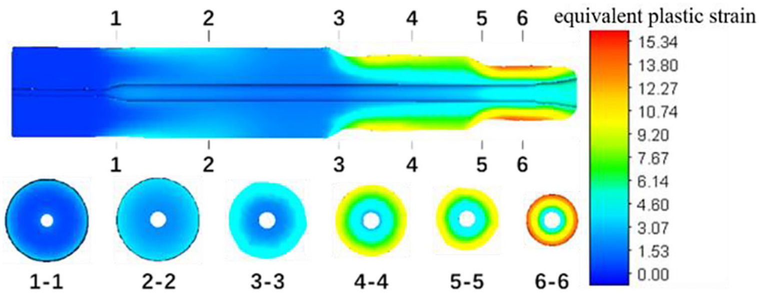

Figure 20. Strain distribution of rolled piece and each section

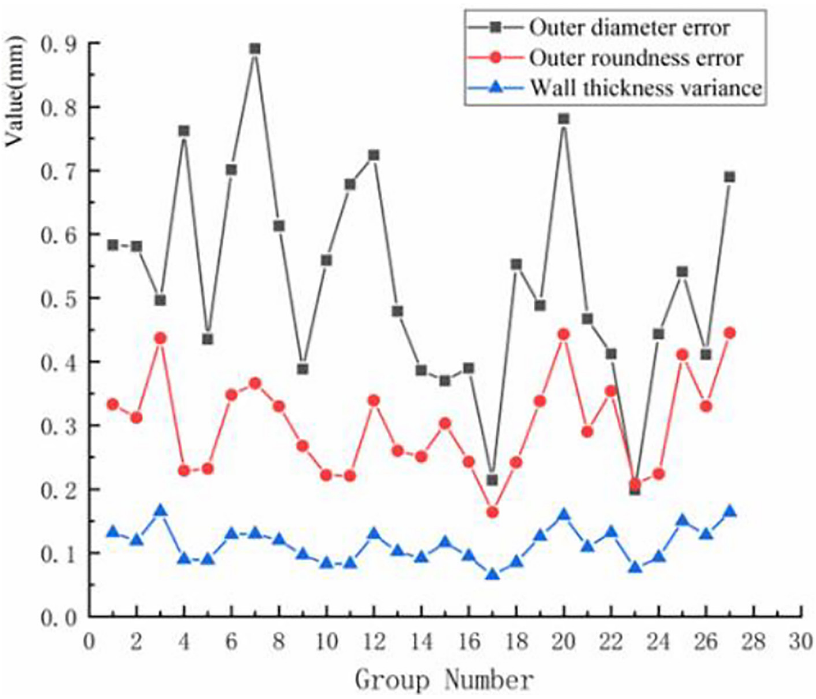

Figure 21. Orthogonal experiment results

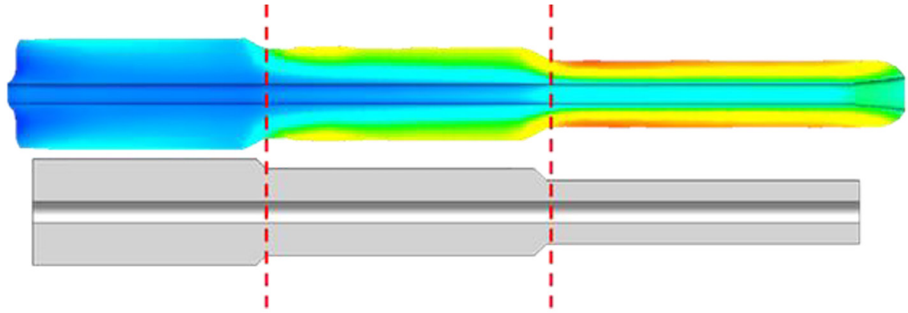

Figure 22. Comparison of simulation results with the shape of the target shaft

Table 3. Simulation results of optimal control parameters

Indicators	Value(mm)
Outer diameter error	0.101
Outer roundness error	0.056
Wall thickness variance	0.021

imported into the data analysis software SPSSAU for range analysis. The optimal surface quality of the rolled piece was obtained when the piercing roll speed was 60 rad/min and feed angle amounted to 8°, the reducing roller 1 speed equaled 90 rad/min and the feed angle was 9°, the reducing roller 2 speed was equal to 130 rad/min, and the feed angle amounted to 12°.

Using the optimal control parameter combination obtained above for simulation, the simulation results compared with the target shaft shape are shown in Figure 22. The overall shape and dimensions met the design requirements of the target shaft, and there were no defects such as twisting, fracturing, or collapsing in the rolled piece, indicating good surface quality of the rolled piece formed by integrated piercing and rolling. The outer diameter size data of the obtained rolled piece were used to calculate the forming quality indicators, and the calculation results are shown in Table 3. This suggests that the indicators of the optimal process parameter combination are all lower than those of the orthogonal experiment group, indicating that the forming quality of the rolled piece obtained with this combination is optimal, thus proving the accuracy of the orthogonal experiment results.

CONCLUSIONS

1. The forging and cutting combination forming process of aeroengine turbine shaft is cumbersome, the deep processing of the inner hole of the long shaft is difficult, the metal fiber cutting reduces the performance, the production efficiency and the material utilization rate are low, and the core technology of precision forging is monopolized.
2. Compared with the forging process, the cross wedge rolling process has the advantages of high efficiency, energy saving and high material utilization rate. However, it is difficult to realize industrialization due to the disadvantages of complex mold design and high equipment cost.
3. Three-roll flexible cross rolling can realize the non-die flexible forming of the turbine shaft outer profile. Variable roll spacing can realize multi-stage long shaft forming to meet diversified parts production, and realize high-efficiency, high-performance, less-cutting and precise volumetric forming of turbine shafts, which significantly improves the material utilization rate.
4. The process of forming aeroengine turbine shaft by short process of piercing and rolling integration combines the hollow billet formed by solid billet piercing with the multi-step shaft shape formed by cross rolling flexible forming, which can realize the synchronous forming of inner hole and outer contour, and can effectively realize the high quality, high quantity and high efficiency production of turbine shaft.

Turbine shafts are typically made from high-temperature alloy materials that possess limited plasticity, high resistance to deformation, a narrow window for hot processing, and poor thermal conductivity. These characteristics lead to an increased dislocation density in the material during plastic forming, making it susceptible to defects. Improvement of the plastic source of heat-resistant superalloy, reducing the dislocation density in plastic deformation, and suppressing the defects that may be generated by plastic deformation are the essential to the successful completion of plastic forming of turbine shaft. The metal flow of the turbine shaft formed by piercing and cross rolling integration (PCRI) is complex. Coordinating and controlling the uniform metal flow in the deformation area is the key to ensure the high-quality forming quality of the process. Therefore, it is necessary to explore the plastic source of plastic deformation of superalloy and its improvement method, establish the theoretical model of rolling collaborative deformation of PCRI process, and establish the macro-micro uniformity principle of synchronous collaborative forming of aeroengine turbine shaft hole shape. It is a series of key scientific problems to be solved urgently to realize the short-process high-quality precision forming of aeroengine turbine shaft PCRI process, and it is the future development direction of turbine shaft precision forming.

Acknowledgements

This research was supported by the National Natural Science Foundation of China [No. 52375346], and the Science and Technology Innovation 2025 Major Project of Ningbo (No. 2022Z064).

REFERENCES

1. Peng Z, Shunming L, Kun X, Gong SQ, Zhan KY, Shen MX, Tian J, Yuan XA. Novel strategy for signal denoising using two-layer SVD and its application to rubimpact fault diagnosis of aeroengine. J. Applied Sciences. 2022; 12: 2342–2342.
2. Bai S. Life prediction method for the combined high and low cycle fatigue of an aero-engine turbine shaft. D. Journal of University of Electronic Science and Technology. 2024.
3. Jang DY, Liou JH. Study of stress development in axis-symmetric products processed by radial forging using a 3D non-linear finite-element method. J. Mater. Process. Technol. 1998; 74: 74–82.
4. Duan SL, Liu JJ. Effect of forging process on wear resistance of GH901 high temperature alloy turbine shaft forgings. J. Hot working technology.2017; 46: 109–112.
5. Tan HB, Dou ZL, Pang SL. Improvement of forging process for GH901 turbine-shaft. J. Forg. Stamping Technol. 2007; 40–42.
6. Liu ZY. Forming process and die design of low-pressure turbine shaft integral forgings. C. Chines mechanical engineering society journal platform. 2002; 4.
7. Wang JP, Zhou DH, Two -step forging process for one GH4169 turboshaft. J. Journal of Shanghai iron & steel research. 2006; 22–32.
8. Ding YF. Machining technology and experimental study on low-pressure turbine shaft of nickel-based superalloy. D. Journal of Xian Shiyou University. 2022.
9. Yao SX, Yang HP. Research on machining processing for a slender turbine shaft. J. Aviation Precision Manufacturing Technology. 2015; 35–38.
10. Wang L, Ha JY, Chen L. Process research of low-pressure turbine shaft. J. New Technology and Products in China. 2016; 43.
11. Chen L, Zhang XX, Wang L, Jiang Y. Research on processing technology of slender hollow turbine shaft. J. New Technology and Products in China. 2016; 40.
12. Ma J. Research on the processing technology of an aero-engine turbine shaft. D. Journal of Chongqing University. 2016.
13. Luo XY. Research on Processing Technology of Aero Engine High Pressure Turbine Rear Shaft. Modern Manufacturing Technology and Equipment. J. 2024; 60: 174–176.
14. Wang SW. Research on process of superalloy turbine rear shaft for aviation. New Technology and Products in China.J. 2014; 124.
15. Jiang XM. Research on deep hole processing technology of hollow long shaft. Aviation Precision Manufacturing Technology. J. 2011; 47: 46–49.
16. Feng YZ, Ding YF, Liu YS, Huang SP. Experimental study on deep hole drilling of GH4169 low-pressure turbine shaft. J. Tool Engineering. 2022; 56: 30–33.
17. Wang H. Research on machining technology for high-pressure turbine rear axle. D. Dalian University of Technology,2020.
18. Luo XY. Research on processing technology of aero engine high pressure turbine rear shaft. J. Modern Manufacturing Technology and Equipment. 2024; 60: 174–176.
19. Jiang XM. Study on machining technology for hollow deep hole. J. Aviation Precision Manufacturing Technology. 2011; 47: 46–49
20. Liu ZZ, Yang DP. Deep hole processing of LW215 screw-turbodrill turbine shaft. J. China Petroleum Machinery. 1996; 60
21. Bulzak T. Multi wedge cross rolling of axle forgings. J. Archives of Metallurgy and Materials. 2023; 68.
22. Zhao XL, Huang YH, Liu SH, Zeng JM, He KH, Xiao G. Study on influencing factors of stacking defects of complex aluminum alloy shaft in multi-wedge cross wedge rolling. J. Hot Working Technology. 2020; 49: 111–113, 116.
23. Shu XD. Multi-wedge synchronous rolling technology and equipment for cross wedge rolling of hollow train shaft. M. Beijing, science press, Chain. 2020; 1, 66–89.

24. Zheng SH. Study on forming and performance theory and experiment of railway hollow shafts in multi-wegde synchrostep cross wedge rolling. D. Ningbo University.2019.
25. Pater Z, Tomczak J. A new cross wedge rolling process for producing rail axles. J. MATEC Web Conf. 2018; 190: 11006.
26. Pater Z, Tomczak J, Bulzak T, Wójcik Ł. Conception of a three-roll cross rolling process of hollow rail axles. J. Forming processing and thermomechanical treatment. ISIJ Int. 2021; 61: 895–901.
27. Pater Z, Tomczak J, Bulzak T. Analysis of a cross wedge rolling process for producing drive shafts. J. The International Journal of Advanced Manufacturing Technology. 2018; 94: 3075–3083.
28. Shu XD, Ye CQ, Wang JT, Xia YX, Zhang S, Wang Y, Xu HJ, Deng YM. Analysis and prospect of precision plastic forming technologies for production of high-speed-train hollow axles. J. Metals. 2023; 13: 145.
29. Shu XD, Zhang S, Shu C, Wang JT, Ye CQ, Xia YX, Essa K, Pater Z. Research and prospect of flexible forming theory and technology of hollow shaft by three-roll skew rolling. J. International Journal of Advanced Manufacturing Technology. 2022; 123: 689–707.
30. Xu YM, Sun BS, Shu XD, Xu HL. Numerical simulation of multi-step turbine shaft in three-roll screw rolling on its influence by diameter reductio. J. Ningbo University. 2021; 34: 55–60.
31. Cheng X, Wang RM, Chen XL, Jin SS, Qian QK, Wu H. An optimized strain-compensated arrhenius constitutive model of GH4169 superalloy based on hot compression. J. Materials. 2024; 17: 3400–3400.
32. Zhang HB, Wang BY, Zhang HJ, Wang X, Wang JP. An internal state variables constitutive model for Ni-based superalloy considering the influence of second phase and its application in flexible skew rolling. J. Journal of Materials Processing Tech. 2024; 118518–118518.
33. Stefanik A, Morel A, Mróz S, Szota PL. Theoretical and experimental analysis of aluminium bars rolling process in three-high skew rolling mill. J. Archives of Metallurgy and Materials. 2015; 60: 157–161.
34. Gryc A, Bajor T. The analysis of influence the parameters of rolling process in three high skew rolling mill of AZ31 magnesium alloy bars on temperature distribution. J. Metalurgija. 2016; 55: 771–774.
35. Pater Z, Bulzak T, Tomczak J. Numerical analysis of a skew rolling process for producing a stepped hollow shaft made of Titanium Alloy Ti6Al4V. J. Archives of Metallurgy and Materials. 2016; 61: 677–682.
36. Pater Z. Analysis of loads and torque in a skew rolling process for producing axisymmetric parts. J. Archives of Metallurgy and Materials. 2017; 62: 85–90.
37. Pater Z, Bulzak T. Tomczak, J. Problems of forming stepped axles and shafts in a 3-roller skew rolling mill. J. Journal of Materials Research and Technology. 2020; 9: 10434–10446.
38. Lin F, Shu XD, Ye CQ. Numerical analysis of integrated forming process of diagonal rolling and piercing of flange nuts. J. Metalurgija. 2023; 62: 81–84.
39. Li YM, Shu XD, Chen Q, Li ZX, Xu HJ, Deng YM. Feasibility analysis of short process flexible precision forming of aluminum alloy automobile hollow shaft. J. Metalurgija. 2024; 63: 35–38.
40. Chen Q, Shu XD, Li YM, Li ZX, Xu, HJ. Piercing-rolling integrated forming process of aero-engine turbine shaft and its numerical simulation and analysis. J. Ningbo University. 2023; 36: 24–29.
41. Chen Q, Research on the integrated forming process of short process multi-roll system piercing and rolling for aircraft engine turbine shafts. Ningbo University, Zheng Jiang, Chain. 2024; to be submitted.